Electrical Homogeneity Mapping of Epitaxial Graphene on Silicon Carbide

Patrick R. Whelan,[†,‡,§] Vishal Panchal,[‖] Dirch H. Petersen,[†] David M. A. Mackenzie,[†,‡]
Christos Melios,[‖] Iwona Pasternak,[⊥] John Gallop,[‖] Frederik W. Østerberg,[#] Peter U. Jepsen,[‡,§]
Wlodek Strupinski,[⊥] Olga Kazakova,[‖] and Peter Bøggild*[,†,‡]

[†]DTU Nanotech and [‡]Center for Nanostructured Graphene (CNG), Technical University of Denmark, Ørsteds Plads 345C,
DK-2800 Kongens Lyngby, Denmark

[§]DTU Fotonik, Technical University of Denmark, Ørsteds Plads 343, DK-2800 Kongens Lyngby, Denmark

[‖]National Physical Laboratory, Hampton Road, Teddington TW11 0LW, U.K.

[⊥]Faculty of Physics, Warsaw University of Technology, Koszykowa 75, 00-662 Warsaw, Poland

[#]Capres A/S, Diplomvej 373, DK-2800 Kongens Lyngby, Denmark

S *Supporting Information*

ABSTRACT: Epitaxial graphene is a promising route to wafer-scale production of electronic graphene devices. Chemical vapor deposition of graphene on silicon carbide offers epitaxial growth with layer control but is subject to significant spatial and wafer-to-wafer variability. We use terahertz time-domain spectroscopy and micro four-point probes to analyze the spatial variations of quasi-freestanding bilayer graphene grown on 4 in. silicon carbide (SiC) wafers and find significant variations in electrical properties across large regions, which are even reproduced across graphene on different SiC wafers cut from the same ingot. The dc sheet conductivity of epitaxial graphene was found to vary more than 1 order of magnitude across a 4 in. SiC wafer. To determine the origin of the variations, we compare different optical and scanning probe microscopies with the electrical measurements from nano- to millimeter scale and identify three distinct qualities of graphene, which can be attributed to the microstructure of the SiC surface.

KEYWORDS: *graphene, SiC, conductivity, terahertz spectroscopy, micro four-point probe, metrology*
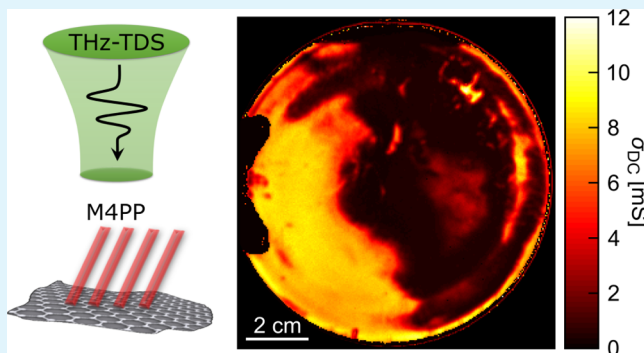
INTRODUCTION

Graphene growth on silicon carbide (SiC) by chemical vapor deposition (CVD) combined with hydrogen intercalation allows 4 in. wafers to be covered with quasi-freestanding (QFS) single-layer graphene (1LG) or bilayer graphene (2LG).[1−5] This technology enhances the carrier mobility and changes the conduction from electrons to holes.[2,6] Precise control of such properties is extremely useful for applications in integrated circuits,[7−9] gas sensors,[10−12] photonics and optoelectronics,[13] and terahertz electronics.[14] However, progress on the development for these types of devices on wafer scale has been limited because of the lack of rapid electrical, optical, and structural characterization techniques capable of imaging entire wafers with spatial resolution ranging from millimeters down to tens of nanometers.[15,16]

Electrical characterization of graphene on SiC has typically required fabrication of Hall bar-type devices, which allow measurements of conductivity, carrier density, mobility, and mean free path.[17] However, these types of devices are sensitive to geometrical errors and material uniformity and provide values that are the weighted average over the device area,[18,19] which can range from micrometers to millimeters square, thus making it difficult and cumbersome to carry out high spatial resolution mapping over larger areas because of inherent inhomogeneities in graphene transport properties.[20] Optical imaging techniques such as optical microscopy and Raman spectroscopy have been successfully used for providing vast information on optical and structural properties, respectively.[21,22] Confocal laser scanning microscopy (CLSM) is an alternative rapid characterization technique for mapping the optical reflection over large areas, while retaining high spatial resolution of ∼150 nm.[23]

There are several techniques that are becoming increasingly popular for studying large areas of two-dimensional (2D)
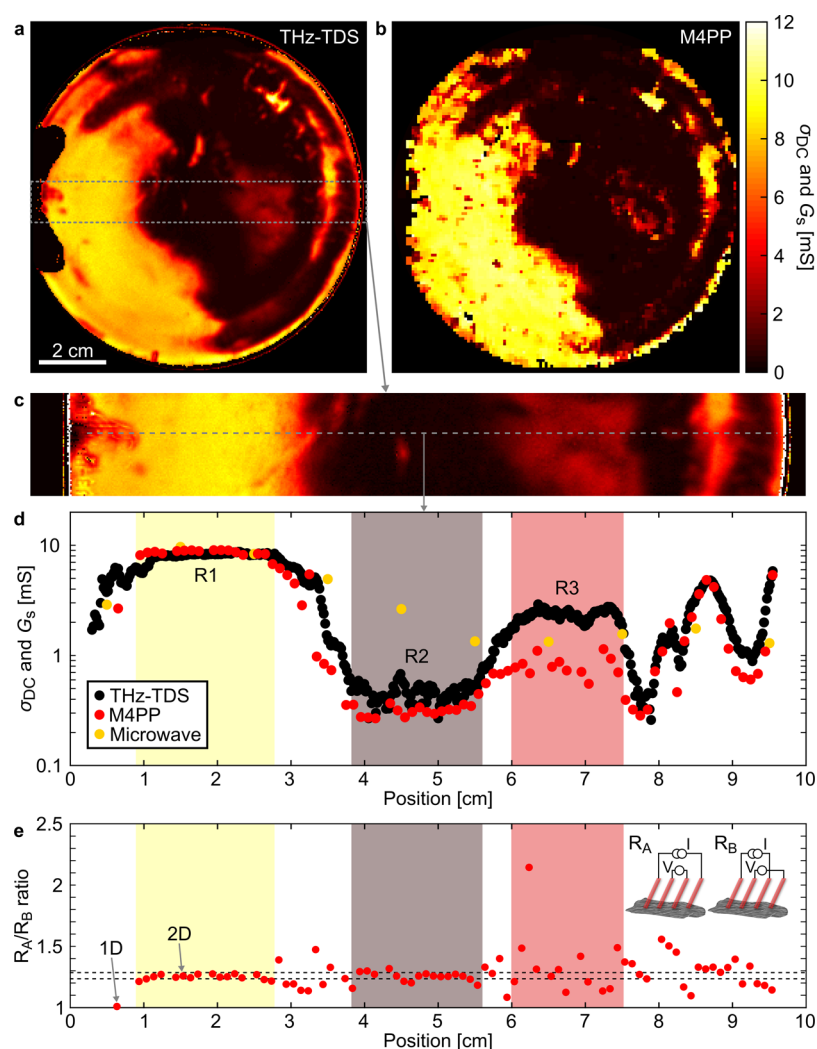
Figure 1. σ_{dc} and G_s map of graphene on a 4 in. SiC wafer measured by (a) THz-TDS (400 μm step size) and (b) M4PP (800 μm step size, 10 μm probe pitch). (c) THz-TDS map of the central region of the wafer (dotted box in (a)) acquired with 200 μm step size. The color bar is the same for (a−c). The M4PP line scan was acquired along the dotted line (1000 μm step size, 350 μm probe pitch). (d) Line plot of σ_{dc} and G_s from THz-TDS, M4PP, and microwave measurements (1 cm step size) following the line in (c). (e) Line plot of the R_A/R_B resistance ratio for the M4PP line scan shown in (d). The dashed lines indicate $\pm 2.5\%$ deviation from a R_A/R_B resistance ratio of 1.26. The insets illustrate the M4PP R_A and R_B configurations.

materials. For instance, terahertz time-domain spectroscopy (THz-TDS), microwave impedance, and micro four-point probe (M4PP) measurements are readily available techniques for mapping the electrical properties of graphene.[24−27] THz-TDS and microwave impedance are contactless techniques, both providing information on electrical conductivity. M4PP measures the electrical conductance on scales from micrometer to millimeter depending on the probe distance, using four electrodes that make direct physical contact to the sample surface. In each of the three cases, maps are generated by scanning a given area of the sample.

In this paper, we combine information from the above-mentioned electrical and optical mapping techniques and reveal significant variations in electrical properties of QFS 2LG across a 4 in. SiC wafer, which we attribute to nanoscale structural variations within the SiC substrate. THz-TDS mapping across the entire wafer reveals order of magnitude variations in the dc sheet conductivity (σ_{dc}). These results are in excellent agreement with M4PP mapping of the sheet conductance (G_s). Although these techniques provide a good

benchmark, they are limited in spatial resolution to tens or hundreds of micrometers and do not reveal the structural properties of graphene and the substrate. Further employing a host of complementary techniques such as CLSM, Raman spectroscopy, atomic force microscopy (AFM), and Kelvin probe force microscopy (KPFM), we observe three distinct areas of graphene characterized by different electrical properties, which we suggest are formed as a consequence of different levels of defects present in the SiC substrate prior to the growth, as also evident by the fact that the same areas are found in same locations on different wafers from the same ingot after growth. The findings here show that the structure and quality of SiC substrates can have drastic impact on the electrical properties of CVD graphene grown on top, even across a single wafer.

■ RESULTS AND DISCUSSION

σ_{dc} and G_s of graphene across a 4 in. SiC wafer were mapped by THz-TDS and M4PP, respectively. The resulting maps (Figure 1a,b) agree well and reveal significant inhomogeneities
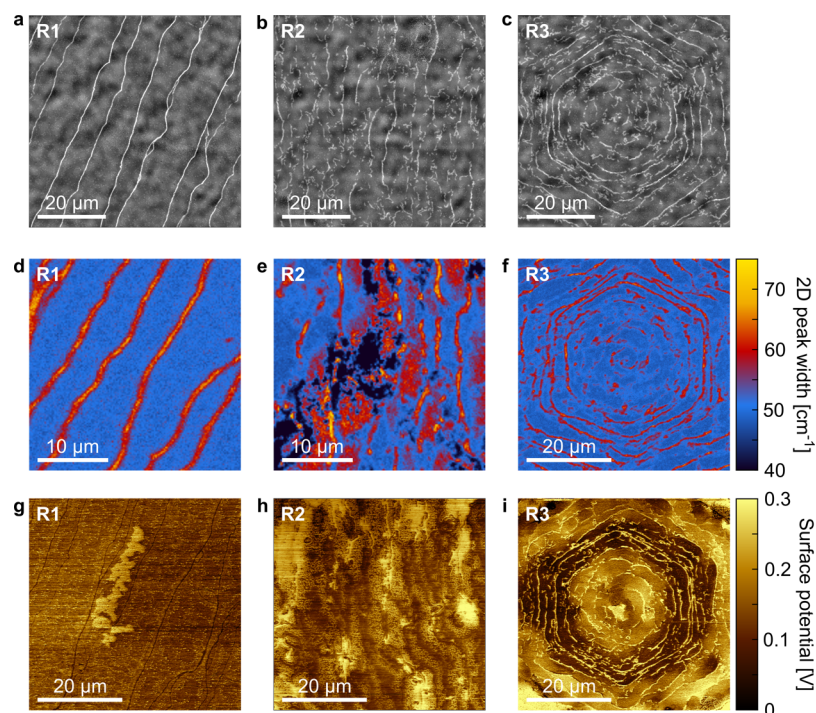
Figure 2. (a−c) CLSM, (d−f) Raman 2D peak width, and (g−i) KPFM surface potential images of graphene on SiC from regions R1, R2, and R3.

in the conducting properties of graphene and highlight variations of more than 1 order of magnitude in σ_{dc} across the 4 in. wafer.

To compare the THz-TDS and M4PP measurements, we performed a higher resolution THz-TDS scan of a stripe across the center of the wafer (Figure 1c). M4PP line scans with larger electrode pitches (150−450 μm) were carried out to achieve a measurement probing a length scale similar to that of the THz-TDS measurement. The THz-TDS σ_{dc} values along the same line were extracted. σ_{dc} and G_s from the line scans are shown in Figure 1d and highlight the excellent correlation between the THz-TDS and the M4PP measurements despite both showing variations of a factor of ~30 across the wafer.

To investigate the reasons behind the variations in σ_{dc} across the 4 in. wafer, we identify three regions of interest (highlighted in Figure 1d) for further studies, R1, R2, and R3. R1 is a region with high and uniform σ_{dc}, where the THz-TDS and M4PP measurements fully agree. R2 is a region with low and relatively uniform σ_{dc}, where the THz-TDS and M4PP measurements also agree. Finally, R3 is a region with intermediate and nonuniform σ_{dc}, where the THz-TDS measurements yield a higher σ_{dc} compared to the M4PP measurements.

G_s extracted from the M4PP line scan is independent of the probe pitch between 150 and 450 μm (Supporting Information Figure S2). Figure 1d also shows the microwave impedance conductivity measured across the same line as the M4PP line scan. σ_{dc} from the microwave impedance measurements agrees quantitatively with the THz-TDS and M4PP measurements in the wide zone R1 but does not track the more rapid spatial variations in R2 and R3 because of the far larger spot size (20 × 20 mm^2).

The M4PP R_A/R_B resistance ratio for the line scan is shown in Figure 1e. In regions R1 and R2, the current flow is 2D-like (~1.26), whereas the R_A/R_B resistance ratio fluctuates in R3, indicating that the current flow is more restricted. This also

explains why the results from THz-TDS and M4PP deviate in R3. THz-TDS is sensitive to the nanoscopic conductivity averaged over a length scale corresponding to the characteristic distance traversed by an electron during one cycle of the alternating THz field, which is on the order of 10−100 nm.[24,25] Given that the spot size of the THz beam is ~350 μm, the measured values of the conductivity can be considered as the average of all 10−100 nm interaction regions across the beam spot, which is essentially the averaged conductivity. In contrast, a M4PP measurement with 300 μm probe pitch (see illustration in Supporting Information Figure S1) is measuring the 2D conductance, which is highly sensitive to any obstructions of the current flow, and only identical to the 2D conductivity for a perfectly uniform conducting film of constant thickness.[24,28,29]

CLSM, KPFM, and Raman spectroscopic mapping were carried out in all three regions, R1, R2, and R3, to further understand the differences in σ_{dc} observed in Figure 1. The CLSM images reveal clear topographical differences between the three regions as shown in Figure 2a−c. In region R1, the sample is highly ordered with large flat terraces and well-defined steps. This corresponds well to the 6H-SiC bulk crystal in regions where the basal plane is tilted less than 0.03° from the (0001) direction. This is known to lead to a well-ordered surface morphology from a step-bunching effect during SiC high-temperature hydrogen etching prior to graphene growth.[1,30] R2 exhibits a less-ordered surface structure, where the terraces and steps are not as well-defined as in R1. This is possibly caused by local plane tilting in the SiC substrate toward various directions.[31] The surface structure of R3 is different to both the previous regions, this time being highly disordered and showing clear signs of screw dislocations. Here, the hydrogen etching of the SiC substrate has formed deep pits.[32] Higher and lower magnification CLSM images from the three regions can be found in the Supporting Information (Figure S3) and show general consistence of images across a

much larger area. On the basis of CLSM images, R3 can contain up to 100 screw dislocations per 1 mm^2 area with the distance between two screw dislocation centers being as low as ~20 μm.

Maps of the Raman 2D peak width (Figure 2d−f) and the surface potential measured by KPFM (Figure 2g−i) corroborate well with the features observed in the CLSM images. However, Raman and KPFM also reveal finer structure on the submicron scale. Representative Raman spectra for R1, R2, and R3 are shown in Supporting Information Figure S4 with average values of the 2D peak widths (full width at half-maximum) for the three different regions summarized in Supporting Information Table S1. The 2D peak widths of 50.5 ± 1.6 cm^{-2} for the blue regions and 59.7 ± 3.3 cm^{-2} for the red/yellow regions in R1 (Figure 2d) are characteristic of 2LG and 3LG, respectively (Supporting Information Figure S4a).[22,33] The structural quality of 2LG is highly uniform for R1 with homogeneous 2LG coverage, where thicker layers of graphene are formed at the step edges. However, the same cannot be said for R2, which shows significant local variations in the 2D peak widths, indicative of nonuniform graphene coverage (Figure 2e). In this region, the average 2D peak widths are 38.1 ± 3.7, 49.8 ± 2.0, and 58.6 ± 3.1 cm^{-2}, which we assign to 1LG, 2LG, and 3LG, respectively (Supporting Information Figure S4b).[22,33] In R3, we observe a similar 2D peak width of 50.1 ± 2.1 cm^{-2} for the blue, 2LG regions, albeit with a slightly larger variation than that of R1 and slightly lower values for red/yellow, 3LG regions, 57.8 ± 2.2 cm^{-2} (Supporting Information Figure S4c). Thus, the structural quality of graphene assessed by Raman spectroscopy in R3 (Figure 2f) is somewhere in-between R1 and R2.

The surface potential in R1 is highly uniform (except for a contaminant object on the surface with higher surface potential, Figure 2g) as opposed to the more strongly varying surface potential in R2 and R3 (Figure 2h,i). In R2, the KPFM image, similar to the Raman 2D peak width, shows local surface potential variations across the surface. The screw dislocations in R3 are also visible in the surface potential image, which varies across individual dislocations. The difference in the surface potential at step edges compared to terraces is higher in R3.

Thus, the distinct indications of disrupted current flow in Figure 1d,e could be explained by the step edges in R3 acting as resistive or reflective barriers obstructing current flow. The step edges are also taller in R3 compared to R1 and R2 (AFM images, Supporting Information Figure S5), which has previously been shown to negatively affect the electrical properties of graphene on SiC.[34−38] The AFM images also show that the terraces between steps in the substrate are flat.

From the detailed CLSM, KPFM, and Raman maps obtained from R1, R2, and R3, it seems clear that the profound differences in the structure of the SiC substrate dictate the growth and corresponding electrical properties of graphene. In R1, we observe a well-ordered topography of the SiC substrate, which leads to the growth of uniform and highly conducting graphene. A graphene layer with strong variations in the surface potential is found in R2, likely originating from the irregular SiC surface structure observed here. Disordered graphene found in R2 has the lowest conductivity across the wafer. In R3, where the THz-TDS and M4PP measurements deviate, we find a high density of screw dislocations with high step edges that seems to affect the current flow. From M4PP measurements conducted inside R3 with a 200 times smaller

pitch (1.5 μm) than in Figure 1 (Supporting Information Figure S6), we find that the variation in G_s across screw dislocations is on the order of the factor of ~30, as also observed across the full wafer. Such large local variations in G_s are bound to lead to variations between THz-TDS (simple spatial average) and M4PP (weighted average between probes) and highlight the complex nature of graphene grown across screw dislocations in R3. Interestingly, the M4PP measurements with small 1.5 μm probe pitch, shown in Supporting Information Figure S6, highlight that G_s in R3 actually contains the same two conductance plateaus as in R1 and R2 and that the intermediate conductivity measured by THz-TDS and M4PP with large electrode pitch in R3 is an average of these. The difference between the measurements originates from the spatial distribution of current flow between electrodes in M4PP measurements being greatly perturbed, whereas the THz-TDS measurement is affected less because it averages over smaller interaction regions across the beam spot.

The claim that the variation in electrical properties of graphene is due to pre-existing defects in the SiC substrate is backed up by a THz-TDS measurement performed on graphene, which was grown on another SiC wafer from the same ingot as the SiC wafer shown in Figure 1. The σ_{dc} map of the second wafer (Supporting Information Figure S7) shows features that are very similar to the map of the initial wafer. The σ_{dc} values are lower for the second wafer, but it clearly shows regions with high and low conductivity that are spatially located at the same areas on the two wafers, thereby supporting the notion that the surface of the SiC substrate is of utmost importance for achieving a homogeneous graphene growth.

■ CONCLUSIONS

THz-TDS and M4PP measurements were performed to map the electrical properties of QFS graphene across a 4 in. SiC wafer. The two measurement techniques are in good agreement and demonstrate how σ_{dc} of the QFS graphene can vary by a factor of ~30 across a wafer. Three distinct regions with specific σ_{dc} behavior were observed. From CLSM, KPFM, and Raman spectroscopy, we find that the differences in electrical properties across the wafer can be attributed mainly to variations in the SiC surface structure that are present prior to graphene growth. The substrate quality, therefore, has a profound impact on the resulting graphene growth. It was found that more defect-free SiC surfaces yield graphene with higher conductivity and with more uniform current flow. The results revealed here give an increased understanding on the crucial importance of the substrate for high-quality growth of graphene on SiC. Additionally, THz-TDS can be used for optimizing the conditions of the graphene growth regardless of the quality of the SiC substrate and for rapidly prescanning of as-grown or QFS graphene samples to identify areas with optimal properties for specific applications.

■ METHODS

Semi-insulating chemomechanically polished SiC substrates were hydrogen-etched prior to graphene growth to remove a few tens of nanometers of the upper SiC, which may have been damaged in the polishing procedure. Etching was performed at 1600 °C and 100 mbar. Epitaxial graphene was subsequently grown by CVD/vapor phase epitaxy on the Si-face of nominally on-axis 6H-SiC in a hot-wall Aixtron G5 reactor commercially used for SiC epi-growth under similar conditions as applied for hydrogen etching, that is, $T = 1600$

°C and P = 100 mbar. Carbon atoms were provided externally by methane delivered to the reactor by an argon carrier gas and deposited (with epitaxy) on the SiC substrate. This method offers the precision of synthesizing a predefined number of carbon layers, including a single layer on the Si-face of SiC.[1,39] With CVD, the nucleation sites for graphene growth are located at the atomic steps, therefore enabling step-flow epitaxy. More details on the growth process can be found in the Supporting Information. The samples were intercalated with hydrogen after growth to decouple graphene from the SiC substrate and obtain QFS graphene.[2,12]

THz-TDS measurements were conducted using a commercial fiber-coupled Picometrix spectrometer.[25] The sample was scanned in the focal plane of a THz beam at normal incidence to form a spatial map with spatial resolution given by the diffraction-limited spot size of ~350 μm at 1 THz (Supporting Information Figure S1). The frequency-dependent sheet conductivity of graphene, $\sigma_s(\omega) = \sigma_1 + i\sigma_2$, can be determined for each pixel in the raster-scanned map through the transmission function $T_{film}(\omega) = E_{film}(\omega)/E_{ref}(\omega)$, where E_{film} and E_{ref} are the Fourier transforms of the THz waveforms transmitted through graphene-covered SiC and nongraphene-covered SiC, respectively. The frequency-dependent sheet conductivity is extracted from the transmission function as[40]

$$\sigma_s(\omega) = \frac{n+1}{Z_0}\left(\frac{1}{T_{film}(\omega)} - 1\right)$$

where Z_0 is the vacuum impedance and n is the refractive index of the SiC substrate.[41] σ_{dc} is extracted, as described previously,[42] by fitting the real part of $\sigma_s(\omega)$ from 0.4 to 1.1 THz to the Drude model, $\sigma_1(\omega) = \sigma_{dc}/(1 - i\omega\tau)$, where τ is the carrier scattering time.

M4PP mapping of G_s was performed on a semiautomatic CAPRES microRSP-M300 using 10 μm electrode pitch, lock-in technique (12 Hz), and a set current of 250 μA. The surface was detected during engagement using a strain gauge sensor to maintain consistent probe pressure and avoid sample damage.[43] Measurements were conducted in two configurations (labeled A and B, see inset in Figure 1e). From the M4PP resistance ratio (R_A/R_B), it is possible to determine whether the current flow in the sample is qualitatively one- or two-dimensional (1D or 2D). If $R_A/R_B = 1$, the current flow is 1D-like, typical for damaged regions where the source-drain current flow is restricted to narrow pathways, whereas $R_A/R_B \approx 1.26$ corresponds to an uninhibited current flow, where the sample is homogeneously conducting in two dimensions.[28,29] The M4PP measurements were conducted with the probes aligned horizontally in all images shown as indicated by the probe positions in Supporting Information Figure S1.

Microwave impedance measurements were carried out to measure the sheet resistivity (R_s) of the graphene film.[44] R_s was determined by measuring the shifts induced to the frequency and quality factor of a sapphire microwave resonator located inside of an electromagnetic cavity. During the measurement, the sample is placed over a 20 × 20 mm^2 opening of the cavity, from which the evanescent near-field emerges. The carriers in graphene interact with the electromagnetic field, thereby shifting the resonance of sapphire, which is measured using a vector network analyzer. R_s can be determined by taking into account the substrate thickness (t_s), permittivity of free space (ϵ_0), relative permittivity of SiC (ϵ_{SiC}), shift in linewidth due to substrate (Δw_s) and graphene (Δw_g), and frequency of the resonator (f_0)[45]

$$R_s = \frac{\Delta f}{\pi f_0 \epsilon_0 t_s (\epsilon_{SiC} - 1)(\Delta w_g - \Delta w_s)}$$

CLSM was performed using an Olympus LEXT OLS4000 system in ambient air.[23] It is designed to operate in reflection mode, and the optical image of the sample was produced by using a photomultiplier tube to capture the reflected optical signal from the 405 nm wavelength laser that is scanned across the sample surface using a micro-electro-mechanical system scanner and galvano mirrors. The system uses a confocal pinhole to eliminate out-of-focus light, which enhances the spatial resolution of the system to ~150 nm. However, using the confocal setup significantly reduces the depth-of-field as the sample plane is often not perpendicular to the optical axis of the microscope objective, with only a small portion of the field-of-view being in focus at a time. A fully in-focus image is achieved by capturing a series of images at different focal-planes along the z-axis (minimum of 60 nm steps) and combining the brightest pixels from each z-stack. This often leads to artifacts, where neighboring brightest pixels from adjacent z-stacks have different brightest intensities.

Raman spectroscopy was performed using a Renishaw InVia system fitted with a 532 nm excitation laser and 1800 groves/mm grating. The laser is focused to approximately 800 nm spot size through a 100× objective (0.85 NA), and the confocality was set to 65 μm slit opening. The maps were acquired in ambient air with 100 nm pixel size, 0.25 s exposure, and ~10 mW laser power. The maps were generated by first normalizing to the highest SiC peak and then subtracting a reference SiC spectra. The G- and 2D-peaks of the resulting spectra were fitted to extract maps for the area, intensity, width, and shift.[22]

Topography (AFM) and surface potential measurements were performed using the Bruker Icon scanning probe microscope in ambient air. The measurements were carried out using a two-pass mode. During the first pass, the topography of the sample was mapped using PeakForce Tapping with PFQNE-AL probes. The PeakForce mode performs force-curves at a rate of 2 kHz and extracts the topography at the specified set point force of 5 nN.[46] In the second pass, the surface potential of the sample was mapped using frequency-modulated KPFM implementation. During the second pass, the probe is kept at a constant lift height of 45 nm by tracing the topography line obtained during the first pass. To measure the surface potential (commonly referred to as the contact potential difference, V_{CPD}), the cantilever is driven on resonance (f_0) while a low-frequency (f_{mod}) ac voltage (V_{ac}) is applied to the conductive probe. This externally applied voltage, together with any other inherent potential differences between the probe and sample, leads to electrostatic attraction/repulsion that shifts the resonance of the cantilever by $f_0 \pm f_{mod}$ and other higher harmonics of f_{mod}. The surface potentials are mapped by using a PID feedback that monitors these side lobes and minimizes them by applying an additional dc voltage (V_{dc}) such that $V_{dc} = V_{CPD}$, thus compensating for V_{CPD} and measuring it at the same time. Further details on FM-KPFM are available elsewhere.[47]

■ ASSOCIATED CONTENT

Ⓢ Supporting Information

The Supporting Information is available free of charge on the ACS Publications website at DOI: 10.1021/acsami.8b11428.

> Schematic representation of measurements; M4PP line scan data; CLSM images; Raman spectra and 2D peak widths; AFM characterization; THz map of the second SiC wafer; and details on graphene growth (PDF)

■ AUTHOR INFORMATION

Corresponding Author
*E-mail: peter.boggild@nanotech.dtu.dk.

ORCID Ⓞ
Patrick R. Whelan: 0000-0002-3978-7029
Christos Melios: 0000-0003-3890-5457
Peter Bøggild: 0000-0002-4342-0449

Notes
The authors declare no competing financial interest.

■ ACKNOWLEDGMENTS

■ REFERENCES

(1) Strupinski, W.; Grodecki, K.; Wysmolek, A.; Stepniewski, R.; Szkopek, T.; Gaskell, P. E.; Grüneis, A.; Haberer, D.; Bozek, R.; Krupka, J.; Baranowski, J. M. Graphene Epitaxy by Chemical Vapor Deposition on SiC. *Nano Lett.* **2011**, *11*, 1786−1791.

(2) Tokarczyk, M.; Kowalski, G.; Możdżonek, M.; Borysiuk, J.; Stępniewski, R.; Strupiński, W.; Ciepielewski, P.; Baranowski, J. M. Structural Investigations of Hydrogenated Epitaxial Graphene Grown on 4H-SiC (0001). *Appl. Phys. Lett.* **2013**, *103*, 241915.

(3) Hwang, J.; Shields, V. B.; Thomas, C. I.; Shivaraman, S.; Hao, D.; Kim, M.; Woll, A. R.; Tompa, G. S.; Spencer, M. G. Epitaxial Growth of Graphitic Carbon on C-Face SiC and Sapphire by Chemical Vapor Deposition (CVD). *J. Cryst. Growth* **2010**, *312*, 3219−3224.

(4) Michon, A.; Vézian, S.; Ouerghi, A.; Zielinski, M.; Chassagne, T.; Portail, M. Direct Growth of Few-Layer Graphene on 6H-SiC and 3C-SiC/Si via Propane Chemical Vapor Deposition. *Appl. Phys. Lett.* **2010**, *97*, 171909.

(5) Liu, Q.; Yu, C.; He, Z.; Gu, G.; Wang, J.; Zhou, C.; Guo, J.; Gao, X.; Feng, Z. Chemical Vapor Deposition Graphene of High Mobility by Gradient Growth Method on an 4H-SiC (0 0 0 1) Substrate. *Appl. Surf. Sci.* **2018**, *454*, 68−73.

(6) Riedl, C.; Coletti, C.; Iwasaki, T.; Zakharov, A. A.; Starke, U. Quasi-Free-Standing Epitaxial Graphene on SiC Obtained by Hydrogen Intercalation. *Phys. Rev. Lett.* **2009**, *103*, 246804.

(7) Tian, H.; Yang, Y.; Xie, D.; Cui, Y.-L.; Mi, W.-T.; Zhang, Y.; Ren, T.-L. Wafer-Scale Integration of Graphene-Based Electronic, Optoelectronic and Electroacoustic Devices. *Sci. Rep.* **2015**, *4*, 3598.

(8) Habibpour, O.; He, Z. S.; Strupinski, W.; Rorsman, N.; Zirath, H. Wafer Scale Millimeter-Wave Integrated Circuits Based on Epitaxial Graphene in High Data Rate Communication. *Sci. Rep.* **2017**, *7*, 41828.

(9) Winters, M.; Sveinbjörnsson, E. Ö.; Melios, C.; Kazakova, O.; Strupiński, W.; Rorsman, N. Characterization and Physical Modeling of MOS Capacitors in Epitaxial Graphene Monolayers and Bilayers on 6H-SiC. *AIP Adv.* **2016**, *6*, 085010.

(10) Cagliani, A.; Mackenzie, D. M. A.; Tschammer, L. K.; Pizzocchero, F.; Almdal, K.; Bøggild, P. Large-Area Nanopatterned Graphene for Ultrasensitive Gas Sensing. *Nano Res.* **2014**, *7*, 743−754.

(11) Varghese, S. S.; Lonkar, S.; Singh, K. K.; Swaminathan, S.; Abdala, A. Recent Advances in Graphene Based Gas Sensors. *Sens. Actuators, B* **2015**, *218*, 160−183.

(12) Melios, C.; Winters, M.; Strupiński, W.; Panchal, V.; Giusca, C. E.; Jayawardena, K. D. G. I.; Rorsman, N.; Silva, S. R. P.; Kazakova, O. Tuning Epitaxial Graphene Sensitivity to Water by Hydrogen Intercalation. *Nanoscale* **2017**, *9*, 3440−3448.

(13) Bonaccorso, F.; Sun, Z.; Hasan, T.; Ferrari, A. C. Graphene Photonics and Optoelectronics. *Nat. Photonics* **2010**, *4*, 611−622.

(14) Yang, X.; Vorobiev, A.; Generalov, A.; Andersson, M. A.; Stake, J. A Flexible Graphene Terahertz Detector. *Appl. Phys. Lett.* **2017**, *111*, 021102.

(15) Yan, H.; Xia, F.; Zhu, W.; Freitag, M.; Dimitrakopoulos, C.; Bol, A. A.; Tulevski, G.; Avouris, P. Infrared Spectroscopy of Wafer-Scale Graphene. *ACS Nano* **2011**, *5*, 9854−9860.

(16) Bae, S.-H.; Zhou, X.; Kim, S.; Lee, Y. S.; Cruz, S. S.; Kim, Y.; Hannon, J. B.; Yang, Y.; Sadana, D. K.; Ross, F. M.; Park, H.; Kim, J. Unveiling the Carrier Transport Mechanism in Epitaxial Graphene for Forming Wafer-Scale, Single-Domain Graphene. *Proc. Natl. Acad. Sci. U. S. A.* **2017**, *114*, 4082−4086.

(17) Yager, T.; Lartsev, A.; Yakimova, R.; Lara-Avila, S.; Kubatkin, S. Wafer-Scale Homogeneity of Transport Properties in Epitaxial Graphene on SiC. *Carbon* **2015**, *87*, 409−414.

(18) Koon, D. W.; Wang, F.; Petersen, D. H.; Hansen, O. Sensitivity of Resistive and Hall Measurements to Local Inhomogeneities. *J. Appl. Phys.* **2013**, *114*, 163710.

(19) Koon, D. W.; Wang, F.; Petersen, D. H.; Hansen, O. Sensitivity of Resistive and Hall Measurements to Local Inhomogeneities: Finite-Field, Intensity, and Area Corrections. *J. Appl. Phys.* **2014**, *116*, 133706.

(20) Mackenzie, D. M. A.; Buron, J. D.; Whelan, P. R.; Caridad, J. M.; Bjergfelt, M.; Luo, B.; Shivayogimath, A.; Smitshuysen, A. L.; Thomsen, J. D.; Booth, T. J.; Gammelgaard, L.; Zultak, J.; Jessen, B. S.; Bøggild, P.; Petersen, D. H. Quality Assessment of Graphene: Continuity, Uniformity, and Accuracy of Mobility Measurements. *Nano Res.* **2017**, *10*, 3596−3605.

(21) Jessen, B. S.; Whelan, P. R.; Mackenzie, D. M. A.; Luo, B.; Thomsen, J. D.; Gammelgaard, L.; Booth, T. J.; Bøggild, P. Quantitative Optical Mapping of Two-Dimensional Materials. *Sci. Rep.* **2018**, *8*, 6381.

(22) Melios, C.; Panchal, V.; Giusca, C. E.; Strupiński, W.; Silva, S. R. P.; Kazakova, O. Carrier Type Inversion in Quasi-Free Standing Graphene: Studies of Local Electronic and Structural Properties. *Sci. Rep.* **2015**, *5*, 10505.

(23) Panchal, V.; Yang, Y.; Cheng, G.; Hu, J.; Kruskopf, M.; Liu, C.-I.; Rigosi, A. F.; Melios, C.; Walker, A. R. H.; Newell, D. B.; Kazakova, O.; Elmquist, R. E. Confocal Laser Scanning Microscopy: A Tool for Rapid Optical Characterization of 2D Materials. arXiv 1804.04420, **2018**.

(24) Bøggild, P.; Mackenzie, D. M. A.; Whelan, P. R.; Petersen, D. H.; Buron, J. D.; Zurutuza, A.; Gallop, J.; Hao, L.; Jepsen, P. U. Mapping the Electrical Properties of Large-Area Graphene. *2D Mater.* **2017**, *4*, 042003.

(25) Buron, J. D.; Petersen, D. H.; Bøggild, P.; Cooke, D. G.; Hilke, M.; Sun, J.; Whiteway, E.; Nielsen, P. F.; Hansen, O.; Yurgens, A.; Jepsen, P. U. Graphene Conductance Uniformity Mapping. *Nano Lett.* **2012**, *12*, 5074−5081.

(26) Mackenzie, D. M. A.; Whelan, P. R.; Bøggild, P.; Jepsen, P. U.; Redo-Sanchez, A.; Etayo, D.; Fabricius, N.; Petersen, D. H. Quality Assessment of Terahertz Time-Domain Spectroscopy Transmission and Reflection Modes for Graphene Conductivity Mapping. *Opt. Express* **2018**, *26*, 9220−9229.

(27) Klarskov, M. B.; Dam, H. F.; Petersen, D. H.; Hansen, T. M.; Löwenborg, A.; Booth, T. J.; Schmidt, M. S.; Lin, R.; Nielsen, P. F.; Bøggild, P. Fast and Direct Measurements of the Electrical Properties of Graphene Using Micro Four-Point Probes. *Nanotechnology* **2011**, *22*, 445702.

(28) Lotz, M. R.; Boll, M.; Hansen, O.; Kjær, D.; Bøggild, P.; Petersen, D. H. Revealing Origin of Quasi-One Dimensional Current Transport in Defect Rich Two Dimensional Materials. *Appl. Phys. Lett.* **2014**, *105*, 053115.

(29) Lotz, M. R.; Boll, M.; Østerberg, F. W.; Hansen, O.; Petersen, D. H. Mesoscopic Current Transport in Two-Dimensional Materials with Grain Boundaries: Four-Point Probe Resistance and Hall Effect. *J. Appl. Phys.* **2016**, *120*, 134303.

(30) Giannazzo, F.; Deretzis, I.; Nicotra, G.; Fisichella, G.; Ramasse, Q. M.; Spinella, C.; Roccaforte, F.; La Magna, A. High resolution study of structural and electronic properties of epitaxial graphene grown on off-axis 4H-SiC (0001). *J. Cryst. Growth* **2014**, *393*, 150−155.

(31) Dimitrakopoulos, C.; Grill, A.; McArdle, T. J.; Liu, Z.; Wisnieff, R.; Antoniadis, D. A. Effect of SiC Wafer Miscut Angle on the Morphology and Hall Mobility of Epitaxially Grown Graphene. *Appl. Phys. Lett.* **2011**, *98*, 222105.

(32) Hannon, J. B.; Tromp, R. M. Pit Formation during Graphene Synthesis on SiC(0001): In Situ Electron Microscopy. *Phys. Rev. B: Condens. Matter Mater. Phys.* **2008**, *77*, 241404.

(33) Grodecki, K.; Jozwik, I.; Baranowski, J. M.; Teklinska, D.; Strupinski, W. SEM and Raman Analysis of Graphene on SiC(0001). *Micron* **2016**, *80*, 20−23.

(34) Yager, T.; Lartsev, A.; Mahashabde, S.; Charpentier, S.; Davidovikj, D.; Danilov, A.; Yakimova, R.; Panchal, V.; Kazakova, O.;

Tzalenchuk, A.; Lara-Avila, S.; Kubatkin, S. Express Optical Analysis of Epitaxial Graphene on SiC: Impact of Morphology on Quantum Transport. *Nano Lett.* **2013**, *13*, 4217−4223.

(35) Nicotra, G.; Ramasse, Q. M.; Deretzis, I.; La Magna, A.; Spinella, C.; Giannazzo, F. Delaminated Graphene at Silicon Carbide Facets: Atomic Scale Imaging and Spectroscopy. *ACS Nano* **2013**, *7*, 3045−3052.

(36) Ji, S.-H.; Hannon, J. B.; Tromp, R. M.; Perebeinos, V.; Tersoff, J.; Ross, F. M. Atomic-Scale Transport in Epitaxial Graphene. *Nat. Mater.* **2012**, *11*, 114−119.

(37) Hollander, M. J.; Agrawal, A.; Bresnehan, M. S.; LaBella, M.; Trumbull, K. A.; Cavalero, R.; Snyder, D. W.; Datta, S.; Robinson, J. A. Heterogeneous Integration of Hexagonal Boron Nitride on Bilayer Quasi-Free-Standing Epitaxial Graphene and Its Impact on Electrical Transport Properties. *Phys. Status Solidi A* **2013**, *210*, 1062−1070.

(38) Bryan, S. E.; Yang, Y.; Murali, R. Conductance of Epitaxial Graphene Nanoribbons: Influence of Size Effects and Substrate Morphology. *J. Phys. Chem. C* **2011**, *115*, 10230−10235.

(39) Strupinski, W. Method of Graphene Manufacturing. U.S. Patent 9,067,796 B2, 2010.

(40) Buron, J. D.; Pizzocchero, F.; Jessen, B. S.; Booth, T. J.; Nielsen, P. F.; Hansen, O.; Hilke, M.; Whiteway, E.; Jepsen, P. U.; Bøggild, P.; Petersen, D. H. Electrically Continuous Graphene from Single Crystal Copper Verified by Terahertz Conductance Spectroscopy and Micro Four-Point Probe. *Nano Lett.* **2014**, *14*, 6348−6355.

(41) Strait, J. H.; George, P. A.; Dawlaty, J.; Shivaraman, S.; Chandrashekhar, M.; Rana, F.; Spencer, M. G. Emission of Terahertz Radiation from SiC. *Appl. Phys. Lett.* **2009**, *95*, 051912.

(42) Buron, J. D.; Mackenzie, D. M. A.; Petersen, D. H.; Pesquera, A.; Centeno, A.; Bøggild, P.; Zurutuza, A.; Jepsen, P. U. Terahertz Wafer-Scale Mobility Mapping of Graphene on Insulating Substrates without a Gate. *Opt. Express* **2015**, *23*, 30721.

(43) Petersen, D. H.; Hansen, O.; Hansen, T. M.; Bøggild, P.; Lin, R.; Kjær, D.; Nielsen, P. F.; Clarysse, T.; Vandervorst, W.; Rosseel, E.; Bennett, N. S.; Cowern, N. E. B. Review of Electrical Characterization of Ultra-Shallow Junctions with Micro Four-Point Probes. *J. Vac. Sci. Technol., B: Nanotechnol. Microelectron.: Mater., Process., Meas., Phenom.* **2010**, *28*, C1C27−C1C33.

(44) Krupka, J.; Strupinski, W. Measurements of the Sheet Resistance and Conductivity of Thin Epitaxial Graphene and SiC Films. *Appl. Phys. Lett.* **2010**, *96*, 082101.

(45) Hao, L.; Chen, J.; Liu, Q.; Gallop, J. Microwave Method for High-Frequency Properties of Graphene. *IET Circuits, Devices Syst.* **2015**, *9*, 397−402.

(46) Pittenger, B.; Erina, N.; Su, C. Mechanical Property Mapping at the Nanoscale Using PeakForce QNM Scanning Probe Technique. In *Nanomechanical Analysis of High Performance Materials*; Solid Mechanics and its Applications; Tiwari, A., Ed.; Springer: Dordrecht, 2014; pp 31−51.

(47) Panchal, V.; Pearce, R.; Yakimova, R.; Tzalenchuk, A.; Kazakova, O. Standardization of Surface Potential Measurements of Graphene Domains. *Sci. Rep.* **2013**, *3*, 2597.